

## 4 DISCUSSION OF RESULTS

An approximation to the real situation is achieved by the construction of a model of the outer layers of the earth. By reducing the complexity of the model I can solve the mathematical equation describing the flexural behavior. The disadvantage of a model is, that I cannot take every parameter into account, even if its influence on the result is relevant. Hence, it is essential to discuss the accuracy of the result. Consequently, I examine the errors of computation resulting from different assumptions and inaccuracy of the input parameters.

### 4.1 THICK PLATE THEORY

All calculations are based on the thin elastic plate theory. This theory assumes that the plate thickness is small compared to its length, perfectly elastic, and the component of stress in the vertical direction is small compared to other stress components and may be set to zero (WATTS 2001).

COMER (1983) derived analytical expressions for the deflections and stresses due to loading of an elastic plate of arbitrary thickness, which he compared with those for thin plate solutions. His thick plate solution is exact for small strains and linear boundary conditions, but in the absence of gravitational forces. He showed that for narrow loads there is a close agreement with the results of thin and thick plate theory. The main disagreements were confined to the region immediately beneath the loads, where the thin plate theory may underestimate the deflection by 5 – 10% .

WOLF (1985) agreed with the results of COMER that for most of the geological situations, the deflection based on the thin plate theory is usually a good approximation. He pointed out some inconsistencies in COMER'S thick plate computation, considering the effect of gravitation. This showed that the differences between the thick and thin plate computation are even smaller than those COMER proposed. The closest correspondence is found for long wavelength loads. However, the thin plate theory is a good approximation to model the deflection of loads (COMER 1986, WOLF 1986 & ZHOU 1991, WATTS 2001).

Also FE-modeling shows the solution for the thick and the thin plate theory is in a good agreement. KWON & BANG (2001) derived a mixed plate bending formulation. They proposed that the major discrepancy between the thick and the thin plate theory is the relation between the rotations and transverse deflection. The consequence is a deviation of about 5% . This is because the shear deformation is negligible if the plate thickness is very small compared to its length.

Conclusively, the thin plate theory is a good approximation to the behavior of the lithosphere and I can assume an error of 5 – 10% .

## 4.2 INFLUENCE OF TEMPERATURE

### 4.2.1 Introduction

From both laboratory and theoretical studies it is known that the rheology of solids is primarily a function of temperature. Therefore, to understand the mechanical behavior of the earth, its thermal structure is considered. In the chapters before I studied the elastic behavior. However, the influence of temperature was not taken into account. In the original differential equation according to Kirchhoff, describing the flexure of an elastic plate, a temperature moment was considered (Chapter 2.1). Unfortunately no comment was found in the literature, whether it is allowed or not to disregard the temperature moment. Therefore in this chapter the influence and significance of the temperature moment will be investigated. Furthermore an application is shown for a typical crustal geotherm in the continental crust given by TURCOTTE & SCHUBERT (2002).

In the following the temperature moment will be considered. For a thickness  $T_e$  of a plate it can be calculated by:

$$m_{\Theta} = \alpha \cdot E \cdot \int_{-\frac{T_e}{2}}^{\frac{T_e}{2}} \Theta \cdot z \cdot dz \quad (\text{see 2.1.3})$$

For  $\Theta$  as the temperature difference related to a situation of no tension due to the heat and  $\alpha [K^{-1}]$  as the coefficient of thermal expansion. For application to the earth's situation I can use a coefficient-value  $\alpha = 10^{-6} \dots 10^{-5} [K^{-1}]$  (PERS. COMM. HUENGES).

### 4.2.2 Synthetic example

In the following I investigate the temperature moment according to a synthetic plate given by GÖLDNER (1978). The point of origin of the Cartesian coordinate system  $x, y, z$  is placed in the central point of the plate whereby  $z$  is directed downwards (Fig. 4.2.1). Given is the Young's modulus  $E [Nm]$ , the elastic thickness  $T_e [m]$  and the distance  $a, b [m]$  relative to the middle point of the plate. The plate (not fixed) is under tension due to a temperature field with  $\Theta = \Theta(z)$ , i.e. the field is constant in the  $x, y$  plane. A temperature distribution

$\Theta = \Theta_0 \left( \frac{z}{0,5 \cdot T_e} \right)$  is assumed. Of course this temperature distribution is not valid for the

Earth's situation. However, this synthetic example is considered in order to calculate the deflection for a given temperature field.

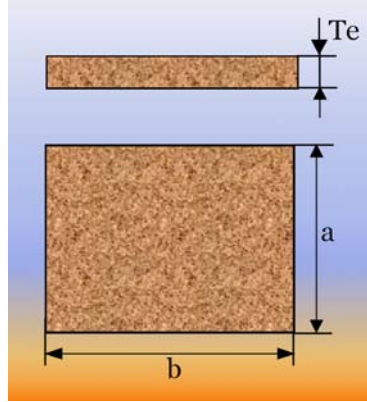


**Figure 4.2.1)** The synthetic example of a plate has a constant elastic thickness.

With this synthetic temperature distribution I can write (see Eq. 2.1.3):

$$m_{\Theta} = \alpha \cdot E \cdot \int_{\frac{-T_e}{2}}^{\frac{T_e}{2}} \Theta_0 \frac{2z}{T_e} z \cdot dz = \alpha \cdot E \cdot \int_{\frac{-T_e}{2}}^{\frac{T_e}{2}} \Theta_0 \frac{2z^2}{T_e} \cdot dz \quad (4.2.1)$$

Solving the integral I obtain:

$$m_{\Theta} = \frac{\alpha \cdot E \cdot \Theta_0 \cdot 2}{T_e} \left[ \frac{1}{3} \cdot \left( \frac{T_e}{2} \right)^3 + \frac{1}{3} \cdot \left( \frac{T_e}{2} \right)^3 \right] = \frac{\alpha \cdot E \cdot \Theta_0 \cdot 2}{T_e} \left[ \frac{2}{3} \cdot \frac{T_e^3}{8} \right] \quad (4.2.2)$$

therefore is:

$$m_{\Theta} = \alpha \cdot E \cdot \Theta_0 \frac{T_e^2}{6} \quad (4.2.3)$$

In view of the fact that the temperature distribution is only a function of the depth, it follows that  $\Delta\Theta(x, y) = 0$  and therefore is  $\Delta m_{\Theta} = 0$ . For this reason it is sufficient to solve the differential equation  $\Delta\Delta w = 0$  (see Chapter 2). According to GÖLDNER (1978) follows for the deflection  $w$ :

$$w = -\frac{6m_{\Theta}}{ET_e^3} (x^2 + y^2) \quad (4.2.4)$$

With use of 4.2.3 I obtain:

$$w = -\alpha \cdot \Theta_0 \frac{(x^2 + y^2)}{T_e} \quad (4.2.5)$$

For the deflection of the corners follows:

$$w = -\alpha \cdot \Theta_0 \frac{(x^2 + y^2)}{T_e} = -\alpha \cdot \Theta_0 \frac{\left( \frac{a}{2} \right)^2 + \left( \frac{b}{2} \right)^2}{T_e} = -\alpha \cdot \Theta_0 \frac{(a^2 + b^2)}{4T_e} \quad (4.2.6)$$

Along with increasing of the dimension of the plate, increase the deflection of the corner points. The deflection of the central point is zero. For  $\Theta_0 = 50K$  and  $\alpha = 12 \cdot 10^{-6} K^{-1}$  (values e.g. GÖLDNER 1978), for the dimension  $a = b = 300000m$  and  $T_e = 30000m$  I can calculate the deflection with:

$$w = -1,2 \cdot 10^{-5} [K^{-1}] \cdot 50 [K] \frac{((3 \cdot 10^5)^2 [m^2]) + (3 \cdot 10^5)^2 [m^2]}{4 \cdot 3 \cdot 10^4 [m]} = 900m \quad (4.2.7)$$

With this given synthetic temperature distribution I would obtain a deflection of  $w = 900m$ . Now I want to investigate the deflection for a given temperature field in the upper layers of the crustal lithosphere.

### 4.2.3 Application in geological sciences

Considering the thermal structure of the Earth, three mechanisms exist for the transfer of the heat: conduction, convection and radiation.

1. Conductive heat transfer occurs through a medium via the net effect of molecular collision. The molecules transmit their kinetic energy to other molecules by collision. Heat is conducted through a medium in which there is a spatial variation of temperature.
2. Convective heat transport is associated with the motion of a medium.
3. Electromagnetic radiation can also transport heat (e.g. radiant energy of the sun). In the Earth, radiative heat transport is only important on a short time scale and its influence can be absorbed into a definition of the thermal conductivity.

The temperature distribution in the continental crust and lithosphere is governed mainly by conductive heat loss to the surface of heat that is generated internally by the decay of radioactive isotopes in the rocks and heat that flows upward from the subcontinental mantle. The basic relation for conductive heat transport is Fourier's law, which states that the heat flux  $q$  (flow of heat per unit area and per unit time), at a point in a medium is directly proportional to the temperature gradient at the point. In one dimension it takes the form:

$$q = -k \frac{d\Theta}{dz} \quad (4.2.8)$$

whereby  $k$  is the coefficient of thermal conductivity and  $z$  is the coordinate in the direction of the temperature variation or depth, respectively. The heat production due to the radioactive elements decreases exponentially with depth (TURCOTTE & SCHUBERT 2002):

$$H = H_0 \cdot e^{-\frac{z}{h_r}} \quad (4.2.9)$$

$H_0$  is the surface heat production rate at  $z = 0$  per unit mass and  $h_r$  is the length scale for the decrease in  $H$  with the depth  $z$ .

## 4.2 INFLUENCE OF TEMPERATURE

At the depth  $z = h_r$  becomes  $H$  an amount  $\frac{1}{e}$  of its surface value. In all cases the length scale  $h_r$  is near  $h_r \cong 10\text{km}$ . TURCOTTE & SCHUBERT (2002, page 143) describe a two-layer model for the continental crust. They obtain a typical geotherm in the continental crust expressed by:

$$\Theta = \Theta_0 + \frac{q_m z}{k} + \frac{(q_0 - q_m)h_r}{k} \left(1 - e^{-\frac{z}{h_r}}\right) \quad (4.2.10)$$

or:

$$\Theta = \Theta_0 + \frac{q_m z}{k} + \frac{(q_0 - q_m)h_r}{k} - \frac{(q_0 - q_m)h_r}{k} e^{-\frac{z}{h_r}} \quad (4.2.11)$$

for the mantle heat flux  $q_m$  and the surface heat flow  $q_0$ . Whereby  $\Theta$  is the temperature and  $\Theta_0$  the surface temperature at  $z = 0$ .

I use this given temperature distribution and solve the integral for the temperature moment. In view of the fact that the temperature distribution is only a function of the  $z$  direction and constant in the  $x, y$  plane I found the same relationship as for the synthetic example. With use of Eq. 4.2.1 and 4.2.11 I obtain:

$$m_{\Theta} = \alpha \cdot E \cdot \int_{-\frac{T_e}{2}}^{\frac{T_e}{2}} \left( \underbrace{\Theta_0}_{const} + \frac{q_m z}{k} + \underbrace{\frac{(q_0 - q_m)h_r}{k}}_{const} - \frac{(q_0 - q_m)h_r}{k} e^{-\frac{z}{h_r}} \right) \cdot z \cdot dz \quad (4.2.12)$$

according to the principal of integral analysis it is allowed to calculate the integral of a sum separately, therefore I can write:

$$m_{\Theta} = \alpha \cdot E \cdot \left( \underbrace{\int_{\frac{T_e}{2}}^{\frac{T_e}{2}} \Theta_0 \cdot z \cdot dz}_{I_1} + \underbrace{\int_{\frac{T_e}{2}}^{\frac{T_e}{2}} \frac{q_m z^2}{k} \cdot dz}_{I_2} + \underbrace{\int_{\frac{T_e}{2}}^{\frac{T_e}{2}} \frac{(q_0 - q_m)h_r}{k} \cdot z \cdot dz}_{I_3} - \underbrace{\int_{\frac{T_e}{2}}^{\frac{T_e}{2}} \frac{(q_0 - q_m)h_r}{k} e^{-\frac{z}{h_r}} z \cdot dz}_{I_4} \right) \quad (4.2.13)$$

with  $I_1 \dots I_4$  as notation for the integral term leads to:

$$m_{\Theta} = \alpha \cdot E \cdot (I_1 + I_2 + I_3 + I_4) \quad (4.2.14)$$

The first integral term  $I_1$  includes a constant term therefore the integral becomes zero:

$$I_1 = \left[ \frac{\Theta_0}{2} z^2 \right]_{\frac{T_e}{2}}^{\frac{T_e}{2}} = \frac{\Theta_0}{2} \cdot \left( \frac{T_e}{2} \right)^2 - \frac{\Theta_0}{2} \cdot \left( -\frac{T_e}{2} \right)^2 = 0 \quad (4.2.15)$$

for the second integral term  $I_2$  is obtained:

$$I_2 = \left[ \frac{q_m}{3k} z^3 \right]_{-\frac{T_e}{2}}^{\frac{T_e}{2}} = \frac{q_m}{3k} \cdot \left( \frac{T_e}{2} \right)^3 - \frac{q_m}{3k} \left( -\frac{T_e}{2} \right)^3 = \frac{q_m}{12k} T_e^3 \quad (4.2.16)$$

The third integral term  $I_3$  is constant and therefore the integral value becomes zero like for the first integral term  $I_1$ . The fourth integral term  $I_4$  is more complex. BRONSTEIN & SEMENDJAJEW (1966) give a solution for  $a$  as a real variable for the following integral:

$$\forall a \in R \quad \int z \cdot e^{az} dz = \frac{e^{az}}{a^2} (az - 1) = F(z) + C \quad (4.2.17)$$

therefore the second term is solved for the  $a = -\frac{1}{h_r}$  and use of Eq. 4.2. 16. by:

$$I_4 = -\frac{(q_0 - q_m)h_r}{k} \cdot \int_{-\frac{T_e}{2}}^{\frac{T_e}{2}} z \cdot e^{-\frac{1}{h_r}z} dz = -\frac{(q_0 - q_m)h_r}{k} \cdot \left[ \frac{e^{-\frac{1}{h_r}z}}{\frac{1}{h_r^2}} \left( -\frac{z}{h_r} - 1 \right) \right]_{-\frac{T_e}{2}}^{\frac{T_e}{2}} \quad (4.2.18)$$

Thus gives:

$$I_4 = -\frac{(q_0 - q_m)h_r}{k} \cdot \left[ h_r^2 e^{-\frac{T_e}{2h_r}} \left( -\frac{T_e}{2h_r} - 1 \right) - h_r^2 e^{\frac{T_e}{2h_r}} \left( \frac{T_e}{2h_r} - 1 \right) \right] \quad (4.2.19)$$

I set  $\mu \equiv \frac{T_e}{2h_r}$  and obtain after multiplication:

$$I_4 = -\frac{(q_0 - q_m)h_r^3}{k} \cdot \left[ -\mu \cdot e^{-\mu} - e^{-\mu} - \mu \cdot e^{\mu} + e^{\mu} \right] \quad (4.2.20)$$

According to BRONSTEIN & SEMENDJAJEW (1966) is:

$$\cosh \mu = \frac{e^{\mu} + e^{-\mu}}{2} \quad \text{and} \quad \sinh \mu = \frac{e^{\mu} - e^{-\mu}}{2} \quad (4.2.21)$$

Therefore Eq. 4.2.20 leads to:

$$I_4 = -\frac{(q_0 - q_m)h_r^3}{k} (-2\mu \cosh \mu + 2 \sinh \mu) \quad (4.2.22)$$

Now  $\mu \equiv \frac{T_e}{2h_r}$  is replaced and from Eq. 4.2.14 follows for the temperature moment:

#### 4.2 INFLUENCE OF TEMPERATURE

$$m_t = \alpha \cdot E \cdot \left[ \frac{q_m T_e^3}{12k} - \frac{(q_0 - q_m) h_r^3}{k} \cdot \left( -\frac{T_e}{h_r} \cosh\left(\frac{T_e}{2h_r}\right) + 2 \sinh\left(\frac{T_e}{2h_r}\right) \right) \right] \quad (4.2.23)$$

according to Eq. 4.2.4. I obtain:

$$w = -\frac{6\alpha(x^2 + y^2)}{T_e^3} \cdot \left( \frac{q_m T_e^3}{12k} - \frac{(q_0 - q_m) h_r^3}{k} \cdot \left( -\frac{T_e}{h_r} \cosh\left(\frac{T_e}{2h_r}\right) + 2 \sinh\left(\frac{T_e}{2h_r}\right) \right) \right) \quad (4.2.24)$$

The deflection is calculated with Eq. 4.2.24 for  $T_e = 1;10;30km$  and the dimension of plate  $x = y = 1...30km$  with  $q_0 = 56.5mW/m^2$ ,  $q_m = 30mW/m^2$ ,  $h_r = 10km$ ,  $k = 3.35W/mK$  (e.g. given by TURCOTTE & SCHUBERT 2002) and  $\alpha = 12 \cdot 10^{-6} K^{-1}$  (PERS. COMM. HUENGES). Fig. 4.2.2 displays the obtained results. A deflection value of  $w \approx 1km$  is obtained at the profile for  $y = 0km$ . Along with the increasing of the elastic thickness increase the amount of the deflection. In the central point located in the origin of the coordinate system the deflection is zero. Along with increasing of the dimension of the plate, increase the deflection.

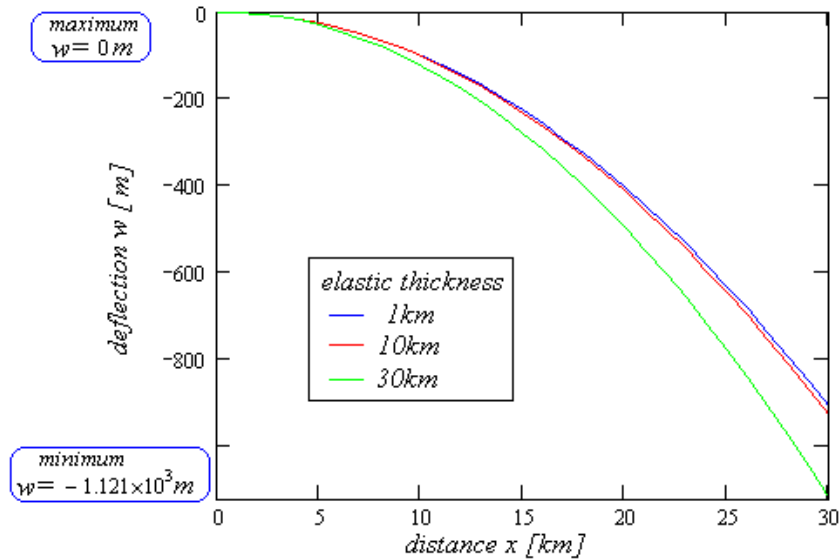


**Figure 4.2.2)** At a profile with  $y = 0km$  the deflection due to a temperature distribution is calculated for a typical crustal geotherm with  $T_e = 1;10;30km$ .

The resulting values of the deflection are significant; therefore it is necessary to consider the temperature moment in the future. The deflection due to the temperature field should be superposed to the deflection due to a load. Therefore heat flux measurements for the special study areas can be used. But the calculation of the temperature moment needs a further investigation and a calibration of the formula. According to these preliminary investigations I can summarize an error in the calculation of the deflection  $\Delta w = \pm 1km$  due to the neglect of temperature (a greater error will occur for an anomalous heat flux).

### 4.3 SIGNIFICANCE OF INPUT PARAMETERS

In order to discuss the error made in the calculation of the deflection  $w$ , I will study the significance of the input parameters. For this purpose it is sufficient to calculate the maximum deflection  $w_0$  with the analytical solution. I want to quantify the dependence of the solution from the input parameters, for this reason I vary the input parameters and investigate the amount of change of the maximum deflection using Eq. 2.3.3 and 2.3.7 (see Chapter 2.3) :

$$w_0 = \frac{P}{8(\rho_m - \rho_k)g \cdot \beta^2} = \frac{\rho_k \cdot g \cdot h}{8(\rho_m - \rho_k)g} \cdot \left[ \frac{ET_e^3}{12(1-\nu^2)} \cdot \frac{1}{(\rho_m - \rho_k)g} \right]^{\frac{1}{2}} \quad (4.3.1)$$

it follows:

$$w_0 = \frac{\rho_k \cdot h}{8(\rho_m - \rho_k)} \cdot \frac{\sqrt{12g(1-\nu^2)(\rho_m - \rho_k)}}{\sqrt{ET_e^3}} \quad (4.3.2)$$

Conclusively, I investigate the influence of the accuracy of the solution with following input parameters: density of crust  $\rho_c$  and mantle  $\rho_m$ , the height  $h$ , the gravity  $g$ , the Poisson's ratio  $\nu$ , the Young's modulus  $E$  and the elastic thickness  $T_e$ .

Deviation [%]	El.Thickness $T_e$ [m]	Poiss.Ratio $\nu$	Gravity $g$ [ $m/s^2$ ]	Young's M.s $E$ [Pa]	Density Mantle $\rho_m$ [ $kg/m^3$ ]	Density Crust $\rho_c$ [ $kg/m^3$ ]	Height $h$ [m]
0	15000	0.25	9.81	1E+12	3300	2750	1000
0.1	15015	0.25025	9.81981	1.001E+12	3303.3	2752.75	1001
0.2	15030	0.2505	9.82962	1.002E+12	3306.6	2755.5	1002
0.5	15075	0.25125	9.85905	1.005E+12	3316.5	2763.75	1005
0.8	15120	0.252	9.88848	1.008E+12	3326.4	2772	1008
1	15150	0.2525	9.9081	1.01E+12	3333	2777.5	1010
2	15300	0.255	10.0062	1.02E+12	3366	2805	1020
5	15750	0.2625	10.3005	1.05E+12	3465	2887.5	1050
8	16200	0.27	10.5948	1.08E+12	3564	2970	1080
10	16500	0.275	10.791	1.1E+12	3630	3025	1100
20	18000	0.3	11.772	1.2E+12	3960	3300	1200
50	22500	0.375	14.715	1.5E+12	4950	4125	1500
80	27000	0.45	17.658	1.8E+12	5940	4950	1800
100	30000	0.5	19.62	2E+12	6600	5500	2000

**Table 4.3.1)** The maximum deflection is calculated for different values of the input parameters. The deviation from the standard values ranges from 0.1%...100% . The standard values are marked in gray.

Hence, a deviation of 0.1%...100% in the standard values (gray marked in Table 4.3.1) results in diverse values, I use for calculation of Eq. 4.3.2 in order to obtain the deviation of the maximum deflection. Only the investigated input parameter is varied and the other input parameters remain constant by using the standard values.

#### 4.3.1 Deviation of height

The resulting maximum deflection for the diverse values for the topographic height is shown in Fig. 4.3.1, the other input parameters remain constant. Logically, the input parameter  $h$  is directly related to the resulting deflection of the plate, i.e. a variation of the height  $h$  by 10% results in 10% deviation in the deflection  $w_0$ .

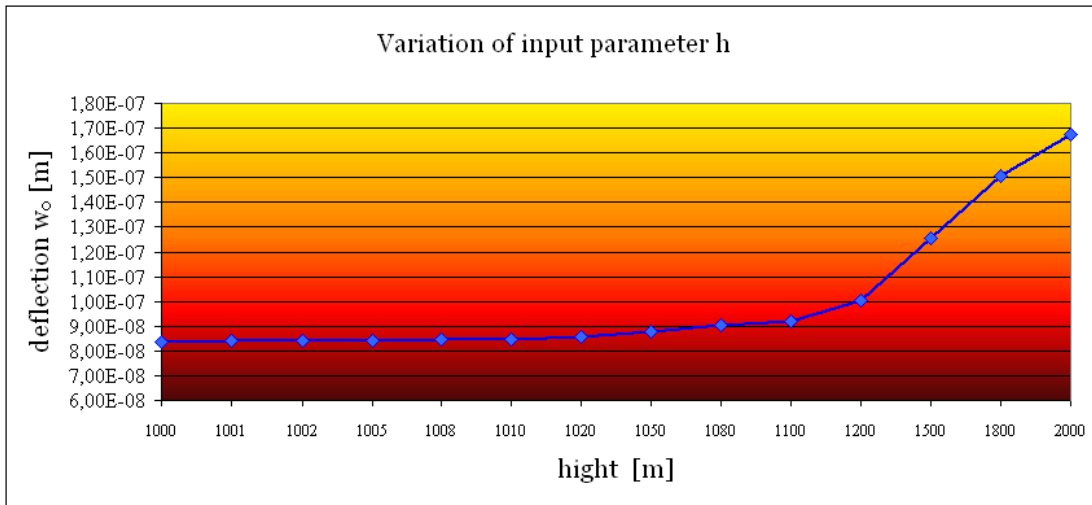


Figure 4.3.1) The deviation of the deflection  $w_0$  was calculated for a variation of  $h$ .

For this reason it is important to consider the accuracy of the height. Generally the input height is given by topography in a DEM grid format (e.g. GEBCO). The inaccuracy of the GEBCO data was investigated by MÜLLER-WRANA. The error of the height was in some cases maximal  $\Delta h = \pm 500m$  (PERS. COMM. MÜLLER-WRANA). In this case I obtain a maximum deflection of  $w_0 = 1.25 \cdot 10^{-7} m$  instead of  $w_0 = 8.5 \cdot 10^{-8} m$ . Because of a standard value  $h = 1km$ , I obtain 50% deviation in the maximum deflection. Consequently the inaccuracy of the height leads to errors in the calculation of the deflection. Therefore it is essential to know the error of the topography/bathymetry grid, because this directly provides the error in deflection. On the other hand the  $T_e/D$  values are obtained by comparing the flexure CMI (due to a topographic/internal load) with the gravity CMI (derived by Bouguer gravity inversion). The main problem is whether or not it is valid to use the Bouguer gravity to estimate the CMI if the present day topography may not be the product of surface or internal loads only. Other factors, such as erosion modify the continental topography, especially at short wavelengths. MCKENZIE & FAIRHEAD (1997) regarded the influence of erosion as significant that they have questioned the validity of  $T_e/D$  estimates based on the Bouguer coherence. Consequently, the estimation by comparison of the gravity CMI and the flexure CMI is questionable as well. However SIMONS ET AL. (2000) explicated, that “erosion

predominantly occurs after the true value of  $T_e / D$  due to loading has left its signature in the gravity and topography field.” This is supported by the fact that the isostatic adjustment to surface and internal loading occurs over a time-scale that is short compared to the long time for erosion (WATTS 2001).

### 4.3.2 Deviation of gravity

The calculation of the maximum deflection for the diverse values of gravity (see Table 4.3.1) is illustrated in Fig. 4.3.2, thereby the other input parameters remained constant. For an input gravity of  $g = 10.0062m/s^2$  I achieve a deflection of  $w_0 = 8.46516 \cdot 10^{-8}m$ . Accordingly a variation of 2% causes a deviation of the maximum deflection of 1% . Hence, the function does not sensitively react to the input parameter of gravity.

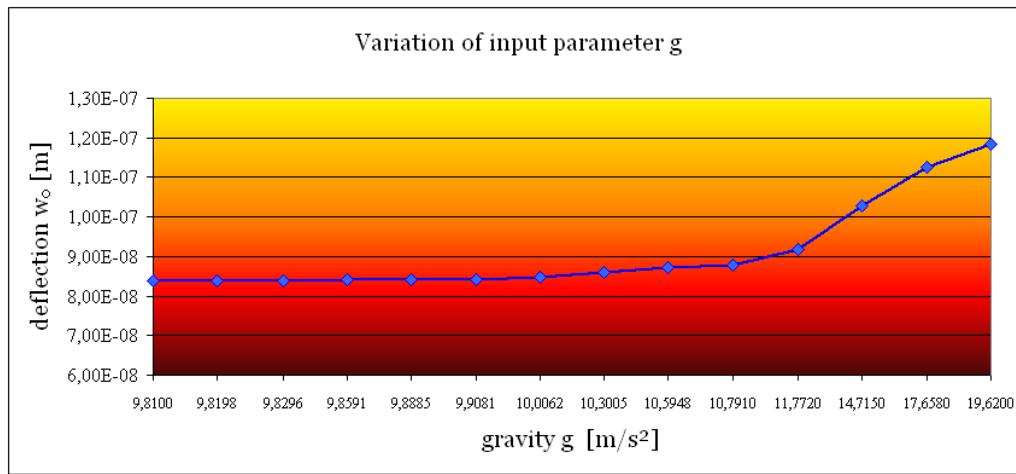


Figure 4.3.2) The deviation of the deflection  $w_0$  was estimated for a variation of  $g$  .

But in the analytical calculation of deflection and therefore in the further estimation of the  $T_e / D$  variation, I operate with a constant gravity value of  $g = 9.81m/s^2$ . However, the gravity is not constant. This leads to the question of the amount of error in deflection made due to this assumption. A gravity value of  $g \approx 9.78m/s^2$  is obtained at the equator for a radius of Earth  $R_{earth} = 6377.4km$ . On the other hand a gravity value of  $g \approx 9.83m/s^2$  is estimated at the North Pole with a radius of Earth  $R_{earth} = 6356.8km$ . Hence I obtain a difference in the gravity value of  $\Delta g \approx 0.03m/s^2$ . An assumed gravity variation of 2% causes a deviation of 1% in maximum deflection. In view of an inaccuracy of less than 1% it is sufficient to operate with a constant gravity value in the analytical computation of deflection or estimation of  $T_e / D$ , respectively.

### 4.3.3 Deviation of Young's modulus

The resulting maximum deflection for the diverse values for the Young's modulus (see Table 4.3.1) is represented in Fig. 4.3.3, the other input parameters remained constant. For an

### 4.3 SIGNIFICANCE OF INPUT PARAMETERS

input Young's modulus  $E = 10^{12} Pa$  I achieve  $w_0 \approx 6 \cdot 10^{-8} m$  for deflection. Thus represents a deviation of about 100% of  $E$ . The deflection changes from  $w_0 \approx 8.5 \cdot 10^{-8} m$  to  $w_0 \approx 6 \cdot 10^{-8} m$ . Accordingly I obtain a difference of  $\Delta w_0 \approx 2 \cdot 10^{-8} m$ , this corresponds to a deviation of 30%. Conclusively, the function is not sensitive to a change of Young's modulus, because 100% deviation of  $E$  cause 30% deviation of  $w_0$ . However, the real problem is, that the parameter of Young's modulus is not exactly estimated. In general a standard value of  $E = 10^{11} Pa$  is used for calculation. However from the other disciplines in geological science is known that the variation of the Young's module is in a range of  $E = 10^9 \dots 10^{12} Pa$ . Therefore an inaccuracy of the Young's modulus  $\geq 100\%$  is probable, this yields to a high error in the calculation of the deflection. Hence, this fact is investigated in Chapter 4.4 more intensively.

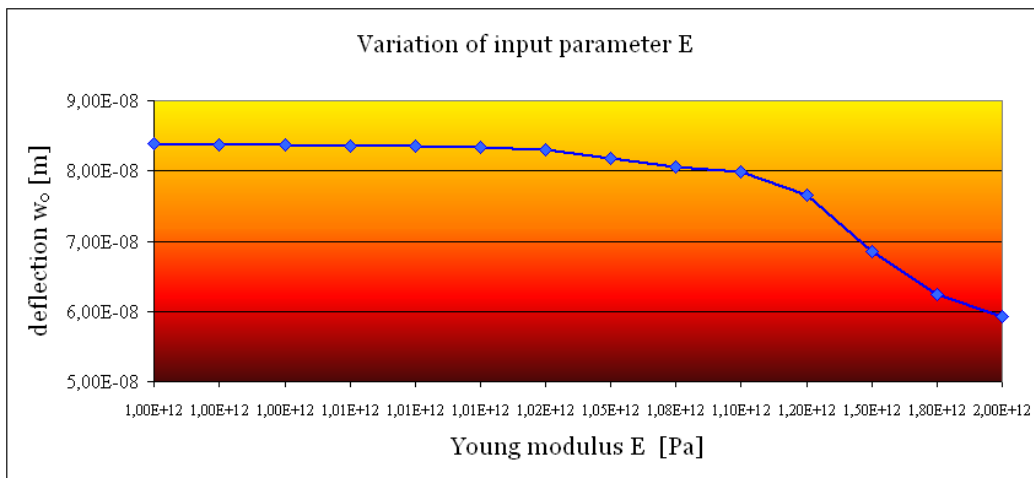


**Figure 4.3.3)** The deviation of the maximum deflection was calculated for different Young's Modulus.

#### 4.3.4 Deviation of Poisson's ratio

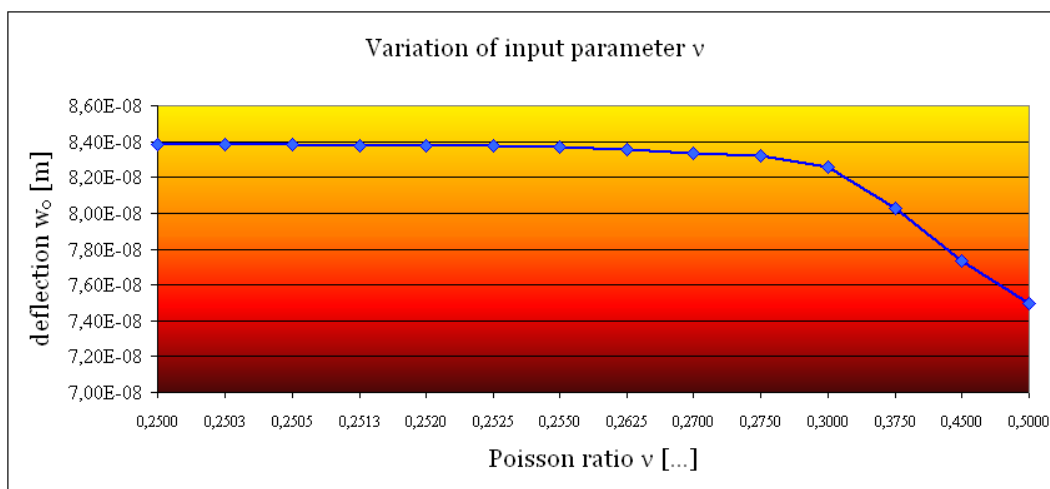


**Figure 4.3.4)** The deviation of the maximum deflection  $w_0$  was estimated for a variation of the Poisson's ratio.

The graph in Figure 4.3.4 represents the maximum deflection calculated for the diverse values for the Poisson's ratio (see Table 4.3.1). The standard values found in literature for the Poisson's ratio vary between  $\nu = 0.25 \dots 0.3$ . This represents a deviation of the input parameter of 20%. This yield to a deflection  $w_0 \approx 8.26 \cdot 10^{-8} m$ , therefore a difference  $\Delta w_0 \approx 4 \cdot 10^{-7} m$ , accordingly  $\leq 1.5\%$  deviation in deflection  $w$ . In view of this fact it is sufficient to operate in the calculation of the deflection with a constant standard value with  $\nu = 0.25$ .

**4.3.5 Deviation of density of crust**

The results of estimation of maximum deflection is presented in Fig. 4.3.5; calculated for the diverse values for the density of the crust (see Table 4.3.1), the other input parameters remain constant.

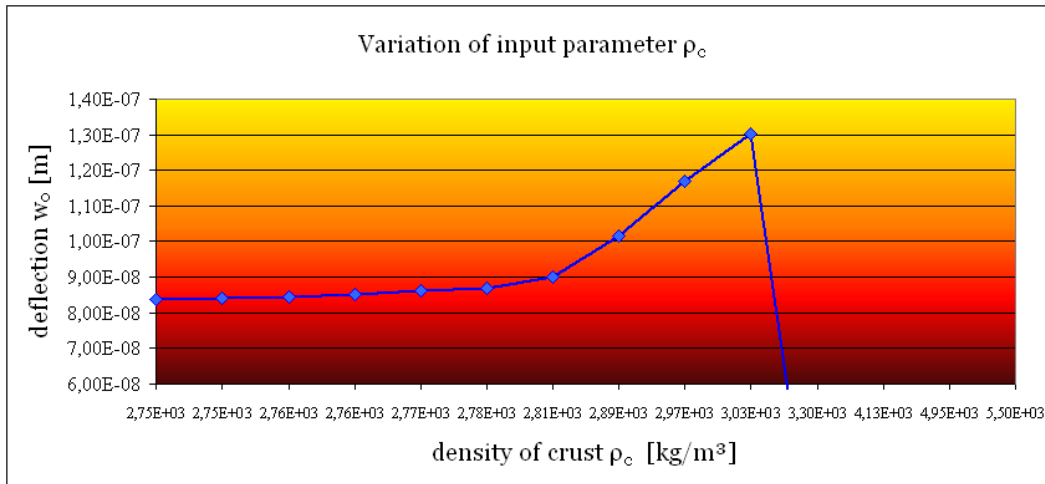


**Figure 4.3.5)** The deviation of the maximum deflection  $w_0$  was calculated for different density values of the crust.

For a density value of  $2800kg / m^3$  instead of  $2750kg / m^3$ , this corresponds to 2% deviation; I obtain a change in deflection of 7.5%. For a density value of  $3030kg / m^3$  the change of deflection becomes large, this is due to the fact, that the solution is dependent from the crust/mantle density contrast. However, in view of the fact that the density value for the crust is estimated with an accuracy of about 2%, an error of 8% has to be taken into account for the deflection  $w$ .

**4.3.6 Deviation of density of mantle**

The resulting maximum deflection is presented in Fig. 4.3.6 for the diverse values for the density of the mantle (see Table 4.3.1). A density value of  $3366kg/m^3$  yields to a deflection of  $w_0 \approx 7.92E-08m$ . Conclusively, for a deviation of 2% of density value of mantle, I estimate a deviation in the deflection of 5.5%. However, the fact that the density value for the mantle is known with an accuracy of about 2%, I have to count with an error of 5.5% for the calculation of the CMI deflection  $w$ .

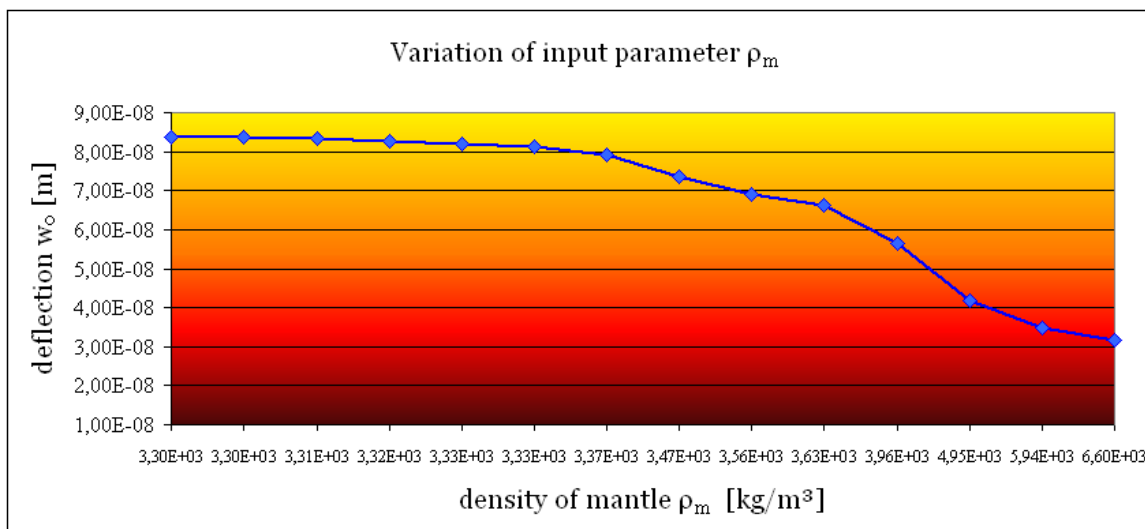


**Figure 4.3.6)** The deviation of the maximum deflection  $w_0$  was computed for different density values of the mantle.

#### 4.3.7 Deviation of elastic thickness

The elastic thickness value is indirectly estimated by comparison of the flexure CMI with the gravity CMI (see Chapter 2.6). Therefore it is essential to estimate the error made due to the inaccuracy in calculation of the deflection (therefore see Fig. 4.3.7). An input elastic thickness value of  $T_e = 17.75km$  instead of  $T_e = 17.00km$  leads to a deflection of  $w_0 \approx 7.79 \cdot 10^{-8} m$ . Conclusively a deviation of 5% from the elastic thickness leads to 7% error in the deflection. And vice versa an error in deflection of 7% leads to an inaccuracy of 5% in estimation of the elastic thickness.

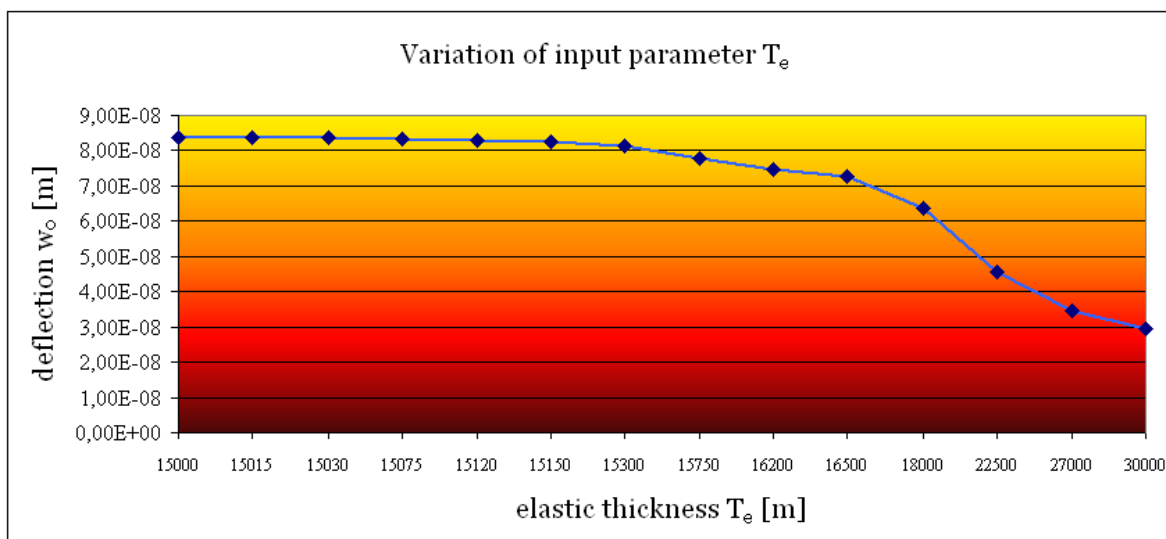


**Figure 4.3.7)** The deviation of the maximum deflection  $w_0$  was computed for different elastic thickness values.

### 4.3.8 Conclusion

Summarizing the results of this chapter I obtain an error in the input parameter, which can be also related to an error in deflection. From the Fig. 4.3.8 I derive the influence of the accuracy of the input parameter to the error in deflection. For example, to guarantee 3% accuracy in computation of deflection, the accuracy in height of 3% , in gravity and in the Young's modulus of 5% , in the density of the crust of 0.8% and in the density of the mantle of 1% is required. However, 2% accuracy of the input parameters for the densities is more realistic. In view of this fact one has to count with an error of about 7% in computation of deflection. I conclude for the indirect estimation of elastic thickness that an error of 7% in deflection leads to an error of 5% in elastic thickness. This means, for example, an elastic thickness value  $T_e = 15km$  has an accuracy of  $T_e = (15.0 \pm 0.8)km$ .

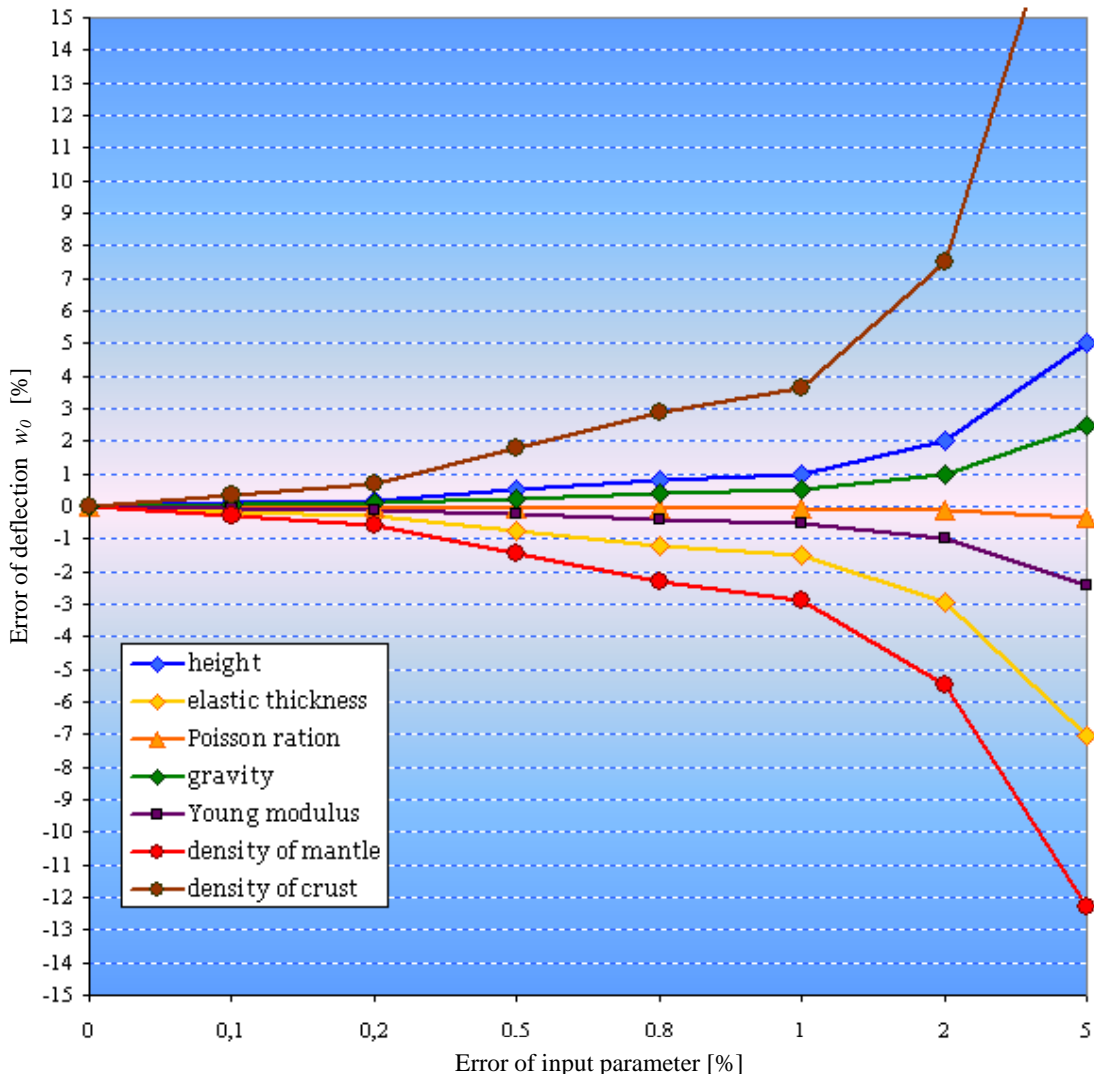


**Figure 4.3.8)** The resulting error of the maximum deflection  $w_0$  is calculated for the deviation of all input parameters.

## 4.4 YOUNG'S MODULUS

The FE models (Chapter 2.7) shows that one of the key parameter controlling deformation is the Young's modulus. Due to the variation in a high order of the Young's modulus the deflection  $w$  is significantly influenced (Chapter 4.3).

A specific value of flexural rigidity  $D$  can be the product of various  $T_e$  values in dependence on the Young's modulus  $E$ . In Figure 4.4.1 displays three curves, which I calculated for a Young's modulus  $E = 10^9; 10^{10}; 10^{11} Pa$  and different elastic thickness values  $T_e$ .

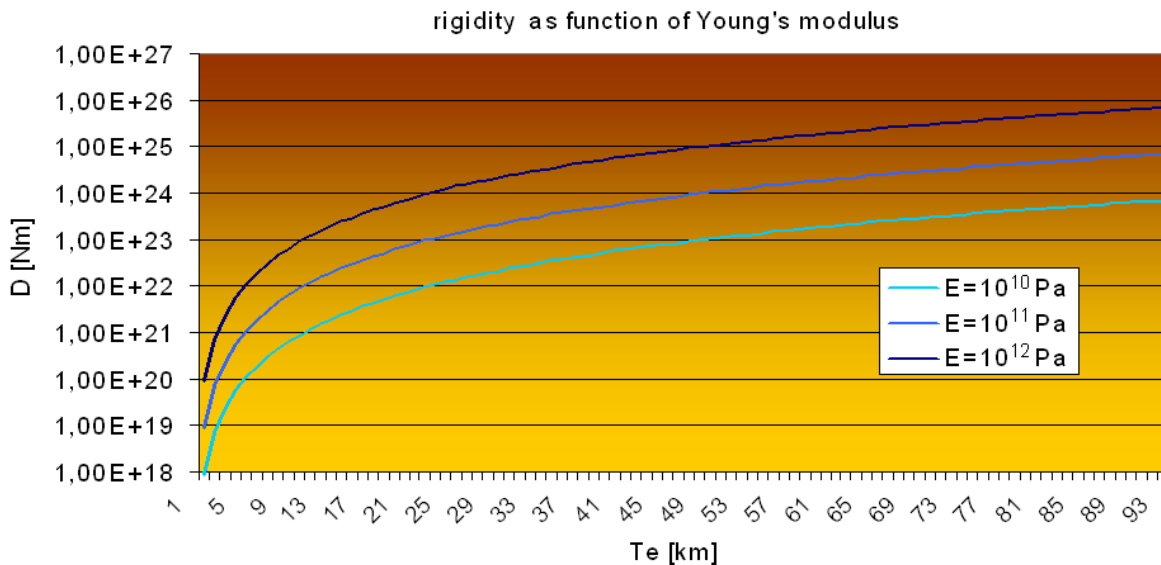


**Figure 4.4.1)** The rigidity is a function of Young's modulus.

The area of the Central Andes is chosen as an example for the following investigation of the significance of the Young's modulus (Chapter 3.2). The importance of Young's modulus is illustrated in Fig. 4.4.2 for calculation of deflection  $w$ . On the one hand, the deflection of the CMI surface in area of Central Andes is calculated for an elastic thickness  $T_e = 30km$  and a Young's modulus  $E = 10^{10} Pa$ . On the other hand, the input parameters are an elastic thickness of  $T_e = 64km$  and a Young's modulus of  $E = 10^{11} Pa$ . In view of the similar CMI depth variation for different Young's modulus results the following idea:

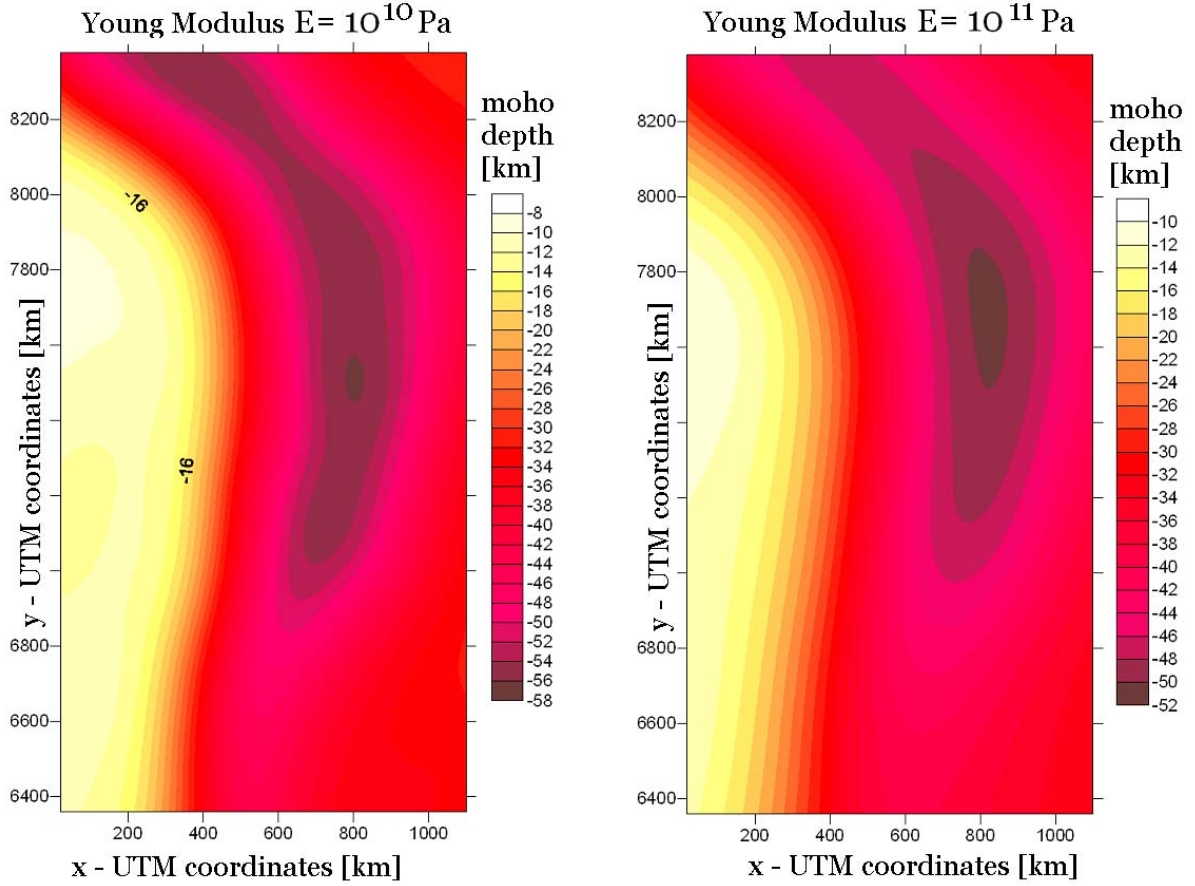


**Figure 4.4.2)** The deflection  $w$  of the CMI depends on the Young's modulus (as example the area of Central Andes is chosen).

In application of the analytical solution the deflection of the CMI is estimated. The spatial variation of the elastic thickness results indirectly.

The fact, that these results were calculated for a constant value of Young's modulus  $E = 10^{11} Pa$  leads to the discussion if the variation of the elastic thickness is obtained or maybe the variation of the Young's modulus (PERS. COMM. KUKOWSKI).

In all methods for estimation of the elastic thickness variation (e.g. admittance, coherence) is always a constant Young's modulus assumed (standard value:  $E = 10^{11} Pa$ ). However, this is not sufficient, as for example sediments are described by a Young's modulus of  $E = 10^9 Pa$  (KUKOWSKI PERS. COMM.). In view of this consideration I transformed the variation of elastic thickness values into a variation of Young's modulus. This has been done for the area of Central Andes (Chapter 3.2). Due to the fact, that the product between the cube of elastic thickness and the Young's modulus is constant:

$$(T_e)^3 \cdot E = c_{i,j} \quad (4.4.1)$$

#### 4.4 YOUNG'S MODULUS

I can recalculate the variation of  $T_e$  values, estimated in the Central Andes for a load model for a constant Young's modulus  $E = 10^{11} Pa$ . Therefore the product can be calculated with:

$$(T_{e_{i,j}})^3 [km^3] \cdot 10^{11} [Pa] = c_{i,j} \quad (4.4.2)$$

If I assume a constant elastic thickness value  $T_e = 40km$  I obtain:

$$(40)^3 [km^3] \cdot E_{i,j} [Pa] = c_{i,j} \quad (4.4.3)$$

Since the results of the Eq. 4.4.2 and Eq. 4.4.3 have to be equal, the variation of elastic thickness  $T_{e_{i,j}}$  in the area of Central Andes can be transformed into a spatial variation of Young's Modulus  $E_{i,j}$  (Fig. 4.4.3).

Therefore it could be formulated, that not a variation of the elastic thickness is observed, but a variation of Young's modulus, thereby the elastic thickness would correspond to the normal crustal thickness.

However, to prove this hypothesis it is necessary to compare the estimated Young's modulus with other results, for example from seismic observation, since Young's modulus is related to a p-wave velocity and a density by:

$$E = v_p^2 \cdot \rho \cdot \frac{(1-2\nu)(1+\nu)}{(1-\nu)} \quad (4.4.4)$$

with the Poissons ratio  $\nu$ . Accordingly the estimated p-wave velocities could be used to compare the results for the variation of the Young's modulus (PERS. COMM. KUKOWSKI & KELLNER). This would go beyond the framework of this study and is a task for investigations in future.

This consideration should illustrate the importance of the Young's modulus. In future examination it is necessary to estimate the Young's modulus in a specific area (e.g. from seismic results). This value could be used as input parameter for estimation of elastic thickness variation for this specific area. Consequently, it is not sufficient to operate with a standard value.

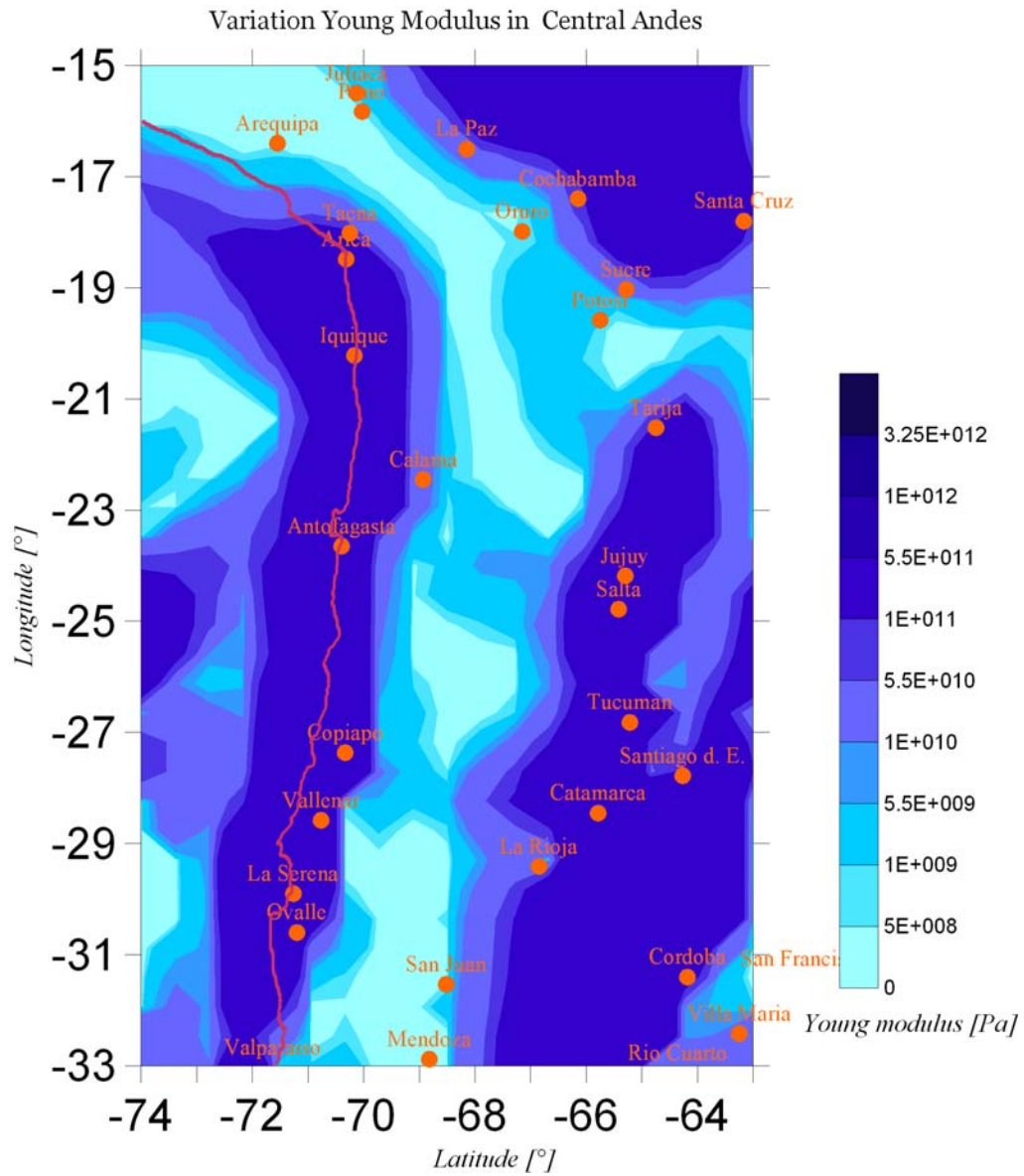


**Figure 4.4.3)** The variation of Young's modulus is calculated for a constant elastic thickness  $T_e = 40km$  in the area of Central Andes.

## 4.5 VISCO – ELASTIC BEHAVIOR

This study demonstrates, that it is possible to explain the observations of flexure in terms of a thin elastic plate model. However, it contains following doubts:

1. The model is very simplistic and provides only a basis for further investigations.
2. The model is time-invariant. It does not take into account the possibility that flexure may change as a consequence of loading.
3. The model predicts exaggerated bending stresses compared with the stress induced by glacial loading and the stress drops observed in earthquakes.

The earth has a variable rheology on different timescales (e.g. RANALLI 1995). It behaves elastically on a very short timescale of seconds to hours, but deforms by viscous flow over long timescales (e.g.  $\geq 10^6$  yr). However, lithospheric rheology at timescales between these extremes is not well understood. Many recent studies of lithospheric rheology and its dependence on time and spatial scales have been encouraged by geodetic measurements that disagree from geological observations (e.g. WERNICKE ET AL. 2000). The discrepancies between geodetic strain and seismic data at convergent plate boundaries may also be explained by different timescales (e.g. WANG 2000). Conclusively, the response of the lithosphere to surface loads does not only depend on size, but also on time scale of loading (see Fig. 4.5.1). For example at the time-scale of seismic surface waves, a few seconds to few hundred seconds, the sub crustal mantle behaves elastically down to very great depths (WATTS 2001).

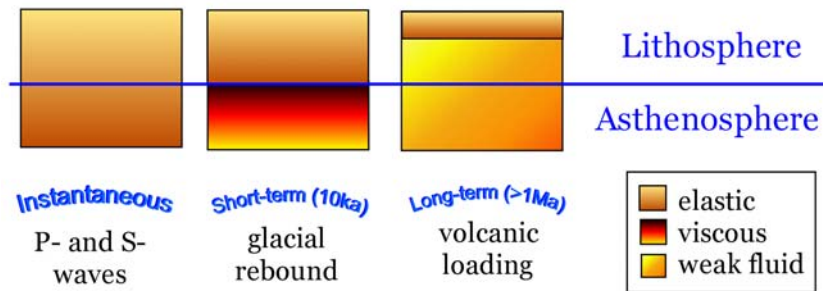


**Figure 4.5.1)** The schematic diagram illustrates the Earth's response to loads of different duration (modified after to WATTS 2001).

Elastic and viscous materials deform in different ways. In the elastic case the applied stress is related to the deformation by Hook's law (see Concepts). In a viscous case the applied stress is related to the rate of change of the deformation with time:

$$\sigma = \eta \cdot \dot{\varepsilon} \quad (4.5.1)$$

whereby  $\sigma$  is the applied stress,  $\eta$  is the viscosity,  $\varepsilon$  is the strain and the dot as subscript indicates a rate, that means the change of strain with time. In opposition to the elastic case, in a viscous case the deformation/deflection will change with time. Maxwell's visco-elastic theory proposes the combination of both, elastic and viscous properties. In view of the

assumption of linearity of the strain the total strain is expressed as the sum of the viscous strain  $\varepsilon_v$  and the elastic strain  $\varepsilon_e$  with:

$$\varepsilon = \varepsilon_v + \varepsilon_e \quad (4.5.2)$$

If it is assumed that the system initially is unstrained, meaning at the time  $t = 0$  is  $\varepsilon = 0$ , then it results:

$$\varepsilon = \frac{\sigma}{E} + \frac{\sigma \cdot t}{\eta} \quad (4.5.3)$$

The time, when the elastic strain that has accumulated is equal to the viscous strain, is described as Maxwell relaxation time and denoted with  $\tau$ . It follows:

$$\tau = \frac{\eta}{E} \quad (4.5.4)$$

WALCOTT (1970) suggested that the flexural rigidity of the Earth's lithosphere is dependent on the load duration. The decrease in rigidity along with increasing duration of loading could generally be described with a relaxation time  $\tau = 0.1Myr$ . In other modeling results (e.g. LIU ET AL. 2002) for the Andes a relaxation time  $\tau = 0.05Myr$  has been used.

Using Eq. 4.5.4 the variation of Young's modulus can be transformed into a variation of viscosities (for example in the Central Andes). The results are presented in Fig. 4.5.2 for a Maxwell relaxation time  $\tau = 0.1Myr$  and  $\tau = 0.05Myr$ . The viscosity values for  $\tau = 0.1Myr$  predominantly range in between of  $10^{23} Pas \leq \eta \leq 10^{25} Pas$ .

Previous investigations of the effective viscosity obtained values in the range in between of  $10^{22} Pas \leq \eta \leq 10^{23} Pas$  (WALCOTT 1970, LOWRY & SMITH 1995, FLESCHE ET AL. 2000). Other modeling results (LIU ET AL. 2002) have shown that the apparently discordant observations of crustal shortening and extension in the central Andes from the GPS, seismological, and geological data can be recompiled by considering the timescale-dependent mechanical behavior of the Andean crust. LIU ET AL. (2002) simulated the nearly elastic behavior of the Andean crust during a short time scale  $\leq 10^2 yr$  with an extremely high viscosity  $10^{25} Pas \leq \eta \leq 10^{27} Pas$  of the various crustal layers. To simulate the long-term crustal shortening in the Andes, they have taken the viscosity of various crustal layers in the range of  $10^{22} Pas \leq \eta \leq 10^{23} Pas$ ; values assumed appropriate for long-term continental deformation (e.g. LAMB 2000). However, the distribution of viscosities in the Central Andes is only an idea to illustrate that a spatial variation of the Young's modulus leads to a variation of viscosity. But the predicted values for the viscosities are comparable with the results mentioned above.

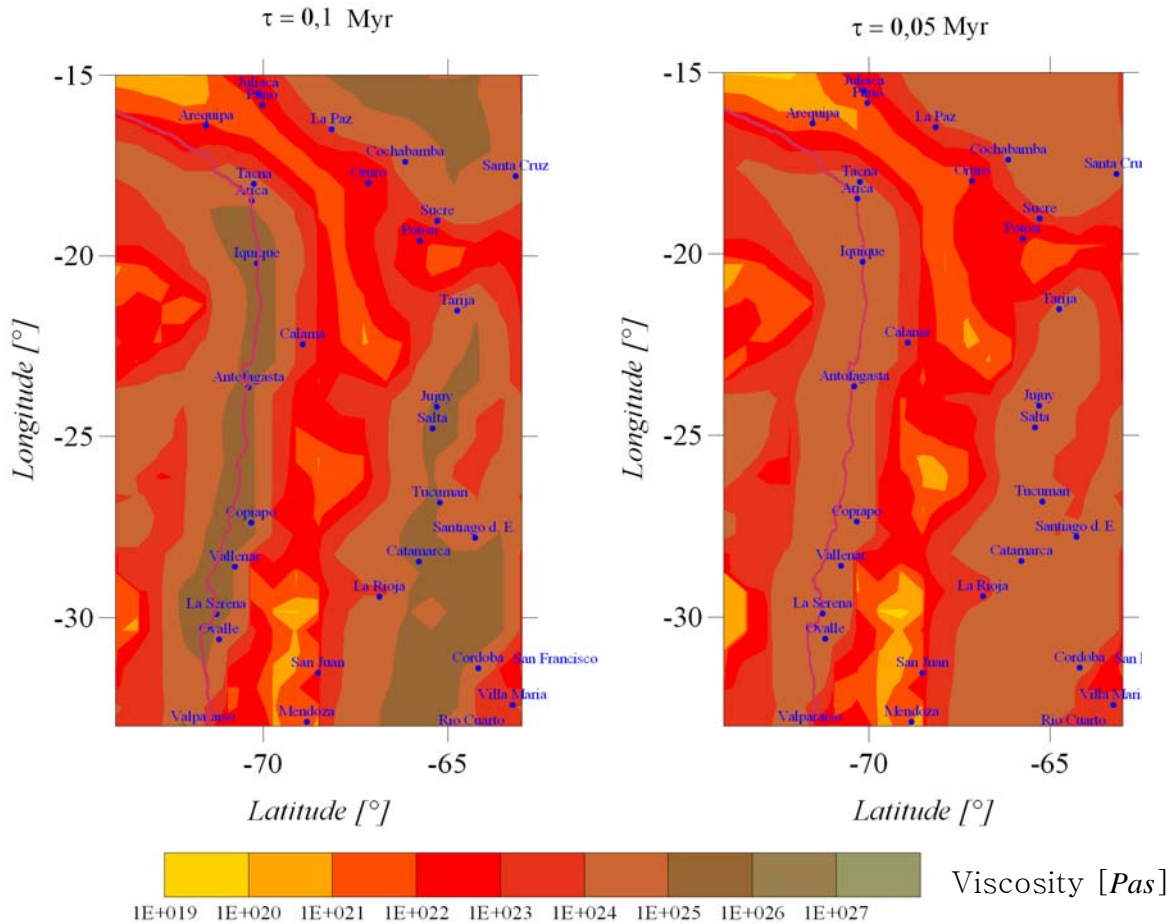


**Figure 4.5.2)** Viscosity distribution  $\eta$  for a Maxwell relaxation time of  $\tau = 0.1\text{Myr}$  and  $\tau = 0.05\text{Myr}$  in the Central Andes derived from Young's modulus variation.

On the other hand the flexure is considered for a specific flexural rigidity value/elastic thickness value. Since deformation of an inelastic medium (plastic, viscous-elastic) can be described as deformation of an elastic medium with time-space variable elastic properties, a deflection of an inelastic plate can be modeled as deflection of an equivalent elastic plate with space-variable  $T_e$  or  $D$ , respectively. This approach, known as the method of elastic solutions, is commonly used in applied mechanics (e.g. GÖLDNER 1978, SCHANZ 1994, ALEXANDROV & POTAPOV 1990).

In view of the fact that the deflection  $w$  increases with time, a lower rigidity value will be obtained, because the time is not considered. Vice versa, for a certain viscosity value a higher rigidity value causes a flexure corresponding in the elastic case to a lower rigidity value (Fig. 4.5.3) . The visco elastic plate equation can be used for investigation of the amount of increasing in deflection with time (and the decreasing of rigidity).

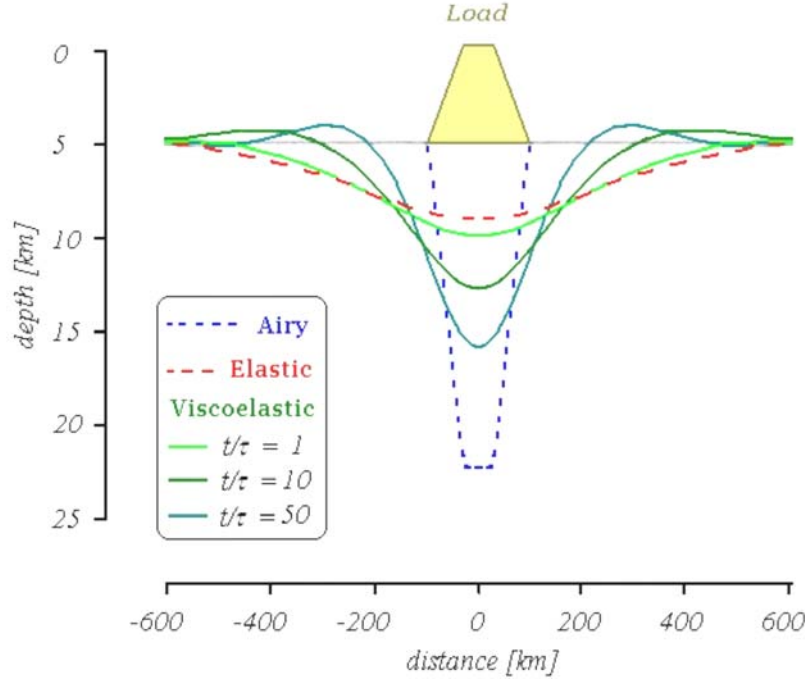


**Figure 4.5.3)** The deflection of a visco-elastic plate was calculated by a narrow two dimensional load. In comparison the flexure curves are calculated for the elastic case for an initial elastic thickness  $T_e = 90\text{km}$  and the Airy compensation. The densities  $\rho_c = 2800\text{kg}/\text{m}^3$ ,  $\rho_w = 1030\text{kg}/\text{m}^3$  and  $\rho_m = 3330\text{kg}/\text{m}^3$  were used for all calculations (modified after WATTS 2001).

The general equation for the flexure of a visco-elastic plate overlaying an inviscid substratum was derived by NADAI (1963):

$$D_0 \frac{\partial^4 w}{\partial x^4} + (\rho_m - \rho_c)g \cdot (\tau \cdot \dot{w} + w) = 0 \quad (4.5.5)$$

whereby  $D_0$  is the flexural rigidity of the visco-elastic plate at  $t = 0$ ,  $w$  is the deflection and  $\dot{w}$  is the derivative of the deflection  $w$  with respect to time. It is useful to consider the response function (WALCOTT 1970):

$$\Phi_V = \frac{1 + \frac{D_0 k^4}{(\rho_m - \rho_c)g} \cdot \left( 1 - e^{-t/\tau \cdot \left[ 1 + \frac{D_0 k^4}{(\rho_m - \rho_c)g} \right]} \right)}{1 + \frac{D_0 k^4}{(\rho_m - \rho_c)g}} \quad (4.5.6)$$

The flexure for a general case of an arbitrarily shaped load for a visco-elastic plate was computed using Eq. 4.5.6. by WATTS (2001).

The flexure was obtained by firstly taking the Fourier transform of the load, multiplying it by the response function and density term, and then take the inverse Fourier transform of the result. This procedure was described in Chapter 2.4. for the elastic case. The graph of flexure is shown in Figure 4.5.3 for the case of a narrow load on the sea floor and different time values of  $t/\tau = 1;10;50$ . The flexure curves are compared with the Airy compensation and the initial elastic case for an elastic thickness  $T_e = 90km$ .

Obviously for an increasing of  $t/\tau$  the maximal deflection  $w_0$  increases. The solution for deflection converges to the Airy response. The visco-elastic model depends on the load: It is different for a narrow and a wide load. In the following the visco-elastic behavior is considered for a narrow load (e.g. load of short wave length of  $\lambda = 100km$ ). The visco elastic plate equation (see Eq. 4.5.5) is highly nonlinear and therefore an exact determination is very difficult. However, it is useful to consider the response function for the elastic and visco-elastic plate. The response function for an elastic plate is given by (Chapter 1.2):

$$\Phi_e = \left[ \frac{D_e k^4}{(\rho_m - \rho_c)} + 1 \right]^{-1} \quad (4.5.7)$$

where  $D_e$  is the flexural rigidity of an elastic plate. Eq. 4.5.6 and Eq. 4.5.7 leads to:

$$D_e = \frac{(\rho_m - \rho_c)g}{k^4} \left[ \frac{1 + \frac{D_0 k^4}{(\rho_m - \rho_c)g}}{1 + \frac{D_0 k^4}{(\rho_m - \rho_c)g} \cdot \left( 1 - e^{-t/\tau \left[ 1 + \frac{D_0 k^4}{(\rho_m - \rho_c)g} \right]} \right)} - 1 \right] \quad (4.5.8)$$

$D_e$  is now the equivalent flexural rigidity of an elastic plate that describes the flexure of a visco-elastic plate.  $D_0$  is the flexural rigidity of a visco-elastic plate at the time  $t = 0$ . The result of this equation is plotted in Fig. 4.5.4. The deflection  $w$  increases with time because the obtained rigidity values decrease with time. For certain values of viscosity and time the corresponding higher value of rigidity can be estimated, which causes the same deflection like a rigidity value which corresponds to the elastic case.

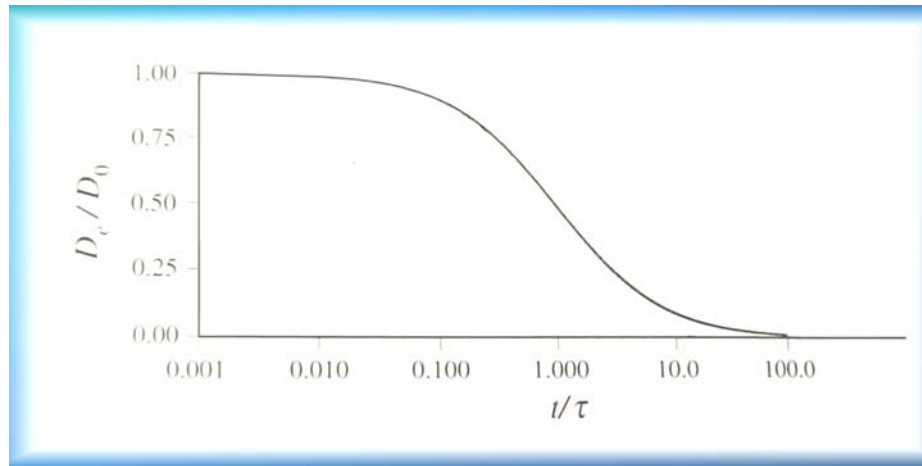


**Figure 4.5.4)** The log-linear plot of the equivalent flexural rigidity of elastic plate  $D_e$  normalized to the flexural rigidity for a visco-elastic plate  $D_0$  was computed for a narrow load at  $t = 0$  (modified according to WATTS 2001).

The ratio is  $t/\tau = 10$  for an assumed time of load with  $t = 1Myr$  (see Fig. 4.5.4). This leads to the ratio  $D_e/D_0 = 0.1$  (it follows:  $D_0 = 10 \cdot D_e$ ). This means that the rigidity would increase to a ten times larger values. The ratio  $D_e/D_0 = 0.5$  is obtained for a time with  $t = 0.1Myr$  which was suggested by WALCOTT (1970). It follows that:  $D_0 = 2 \cdot D_e$ , which means that the rigidity would become two times larger.

For a short duration of load with  $t = 0.0001Myr$ , i.e.  $t/\tau = 0.001$  is the relation  $D_e/D_0 = 1$ . Consequently, the estimated values for rigidity/elastic thickness are valid for a short time of loading with  $t = 0.0001Myr$  and a relaxation time  $\tau = 0.1Myr$ .

## 4.6 FINAL COMMENTS AND FUTURE DIRECTIONS

Vening-Meinesz introduced the concept that the flexural strength of the lithosphere had to be taken into account for isostatic consideration. Many methods have been developed for the estimation of the flexural strength of the lithosphere. I introduced the differential equation describing the flexure of a thin plate (see Chapter 2.1), which was so far not analytically solved for any irregular shaped topography. For a homogeneous isotropic elastic plate the problem had been treated in the frequency space. The disadvantage of the spectral methods motivated the search for an analytical solution of the differential equation.

The newly derived analytical solution was compared with the solutions achieved by the Fast Fourier transformation techniques. Furthermore, if introducing a new solution, it has to fit well into accepted theories, wherefore boundary cases were considered. For a small  $T_e / D$  value, the analytical solution converges to the solution according to Airy. For a high  $T_e / D$  value, the undulation becomes smaller and the CMI surface converges to a plane of constant depth. These results give further evidence of the correctness of the analytical solution.

It became possible with the analytical solution to compute the CMI undulation or the lithosphere/asthenosphere boundary for any irregular shape of topography. Additionally, it gives us some insight into the "black box" of the calculation process.

The question whether the deflection of the crust/mantle boundary or the deflection of the lithosphere/asthenosphere boundary is considered depends on the depth at which the Young's modulus changes (see chapter 2.7). I can interpret the general concept of calculation of a flexure, that the calculated flexure-surface is shifted with the reference depth at the depth where the change of Young's modulus is assumed. Therefore, the calculated flexure is valid for both the crust/mantle interface and the lithosphere/asthenosphere boundary. Furthermore, we conclude that the change of the Young's modulus controls the type of deformation. Except for uncertainties due to operating with a constant E value, the elastic thickness/rigidity is estimated with an accuracy of 5% (see chapter 4.3).

In the following the results of this work are summarized and compared with the developed ideas and concepts of the members of the SFB 267 ([HTTP://WWW.FU-BERLIN.DE/SFB267](http://www.fu-berlin.de/sfb267)).

The rigidity/elastic thickness distribution was estimated for different areas of the Pacific Ocean, in particular for the Nazca and a part of the Antarctic oceanic lithospheric plate, and for the continental lithospheric plate in the northern area of the Central Andes and the Patagonian Andes in the South. The results of the spatial  $T_e / D$  variation are presented as an overlay over the topography in Figure 4.6.1.

The northern and southern parts of the Andes are extremely variable concerning width, altitude, climatic and mechanical properties. The topographically low Patagonian Andes are contrasted with the broad and high Central Andes. During the Cenozoic the world second-largest plateau, the Altiplano/Puna, developed in the Central Andean Cordillera. The formation of this plateau was investigated by the members of the SFB focusing on the

influence of crustal shortening, magmatic addition, mantle delamination and hydration. Both areas are characterized by very different tectonic styles in the backarc. As consequence of large amounts of shortening the fold and thrust belt in the Central Andes is widespread and thin- to thick-skinned. In the area of the Patagonian Andes, a narrow thrust belt with minor shortening can be found. In the northern area, the SFB community found out that a crustal shortening of  $\approx 250\text{km}$  had taken place since Miocene time. They also discovered that the volcanic front of the Coastal Cordillera had migrated to its present position in the Western Cordillera since the Jurassic. While the volcanic front in the Central Andes migrates  $\approx 200\text{km}$  eastward, its position remained almost stable in the southern Andes. In the Patagonian Andes, no plateau developed despite of similar boundary conditions regarding the plate tectonic situation. The crustal thickness of the southern part of the Andean orogen decreases from  $\approx 70\text{km}$  to  $\approx 40\text{km}$ . Also, the depth of seismicity in the Wadati-Benioff zone decreases from  $\approx 660\text{km}$  in the north to  $\approx 100\text{km}$  in the south. Furthermore, the climatic conditions are different in the Central and Patagonian Andes.

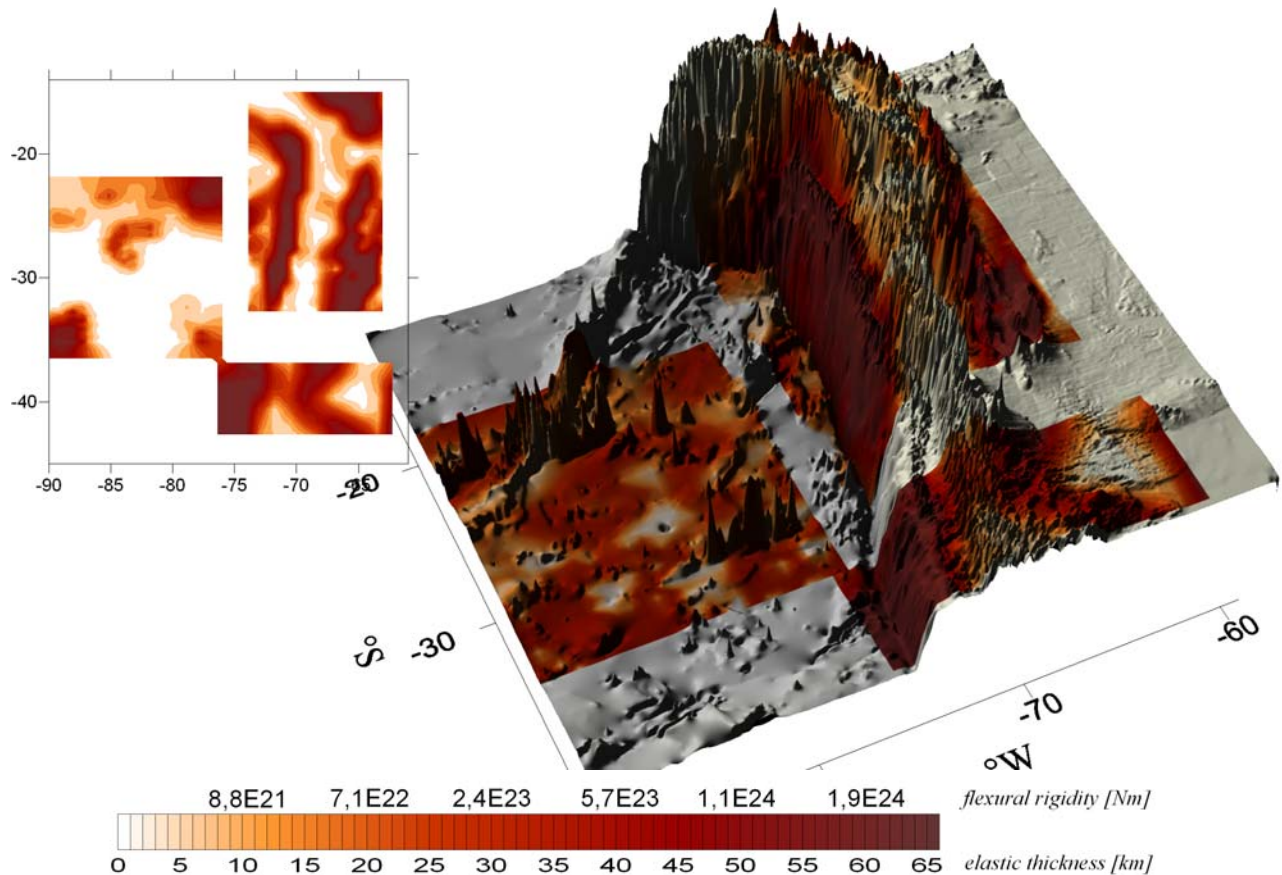


**Figure 4.6.1)** All results of rigidity/elastic thickness in the Pacific Ocean with a reference depth of  $28\text{km}$ , the Central Andes in the northern part ( $30\text{km}$ ) and the Patagonian Andes in the southern part ( $30\text{km}$ ) are summarized. The top view shows the rigidity distribution for the same reference depth of  $30\text{km}$ .

As a result of many discussions, the members of SFB 267 community have identified a number of phenomena expected to be important key parameters for controlling subduction related orogeny and plateau development:

1. The role of stress coupling and force transmission across convergent plate boundaries, as well as the controversial nature of the strength of plate boundaries
2. The properties of subducting oceanic slabs with the related impact on the thermal structure of the deep parts of the system
3. The role of the mantle lithosphere and its degree of stability during orogeny
4. The influence of melts in weakening crustal materials
5. The influence of inherited structures in the upper plate on deformation partitioning

In the following, these results are compared with the results of this proposed study.

- (1) By comparing the results of the oceanic plate rigidity distribution for a reference depth of 30km, a northern rigid part is obtained in contrast to a southern weak part, described by lower rigidity values. In view of the observed difference in the strength of the subducted oceanic plate, this key parameter is confirmed.
- (2) I concluded the importance of the temperature distribution from the deflection of the lithospheric plate due to a temperature moment (see chapter 4.2). In view of the fact that an orogen converges to a state of equilibrium the consideration of the temperature distribution is essential. Therefore, the influence of the colder oceanic slab on the thermal structure of the mantle should be significant to cause a difference in the mechanical behavior of the lithosphere.
- (3) The obtained lower rigidity values in the area of the Altiplano/Puna plateau correlate with the idea of delamination of the mantle lithosphere. Furthermore, a delamination of the upper mantle can be described by a change in the Young's modulus. Regarding the FE models (Chapter 2.7) it was concluded that for an equal  $E$  the deformation and flexure of two layers can be considered as one single plate. Therefore, the crust and upper mantle are coupled and behave mechanically like one lithospheric plate. With a decrease of the Young's modulus in the mantle (e.g. due to increasing temperature) the mechanical behavior completely changes.
- (4) The influence of melts is significant for the rigidity of the lithosphere. Additionally, fluids and melts lead to a decrease in the Young's modulus, which was proposed to be the crucial factor for lithospheric deformation.
- (5) The inherited structures can be described physically by a change in Young's modulus or rigidity, respectively. A very good correlation of the rigidity distribution with the tectonic structures and fault systems could be obtained (see chapter 3 and 4.4). This fact supports their influence on the mechanical deformation.

Usually, low rigidity values are obtained in the inner mountainous basins compared to higher values in the back-arc region. This coincides well with the results of the distribution of

electrical resistivity (PROJECT G4, BRASSE & HAAK 2002) from magneto-telluric investigations and the analysis of surface waves (PROJECT F3, SHAPIRO ET AL. 2002).

In the area of the Central Andes the most geophysical features are probably caused by fluid- and melt associated petrologic processes driven by active subduction (SFB 267). The observation indicates a presence of partial melt or metamorphic fluids at a mid-crustal level beneath the Altiplano-Puna plateau (e.g. PROJECT G3, KIND ET AL. 2002). This observation is in agreement with the analysis of the rigidity distribution, which indicates a mechanically very weak plateau.

The obtained high rigidity values eastwards of the orogen indicate a mechanically strong body correlating with the location of the Brazilian Shield, which is known as a cold and rigid craton. This rigid body is assumed to play an important role in the plateau formation. This correlates well with the results of the numerical models (PROJECT F2, KLOTZ 2002), which suggest that the crustal thickening in the area of Central Andes is caused by underthrusting of the Brazilian shield. In the applied viscous flow model the viscosity was constraint between  $\eta = 10^{24} \dots 10^{18} \text{ Pas}$ , which is comparable with the results in Chapter 4.5 for the viscosity variation.

This work aims to explain the meaning of the elastic thickness as well as the flexural rigidity. The parameter that characterizes the apparent flexural strength of the lithosphere is the flexural rigidity  $D$ , which was commonly expressed through the elastic thickness  $T_e$  of the lithosphere. In the past, standard values were used for the Poisson's ratio and the Young's modulus; this is sufficient for the Poisson's ratio but not for the Young's modulus (see chapter 4.3 and 4.4). As a conclusion the variation of the Young's modulus can be in order of  $E = 10^9 \dots 10^{12} \text{ Pa}$ . Therefore, the physical meaning and significance of the elastic thickness are still enigmatic.

In the example of Central Andes the  $T_e / D$  distribution was transformed into a Young's modulus variation. By assuming a constant  $T_e$  value, which corresponds to an average crustal thickness,  $T_e = 40 \text{ km}$  a meaningful variation of  $E$  was obtained. Therefore, a new definition for the elastic thickness can be formulated.

A new interpretation of the elastic thickness could be that a pseudo-variation is observed because of using a constant standard value for the Young's modulus. The elastic thickness could correspond to the crustal thickness. This is supported by the mathematical fact and physical background that the initial differential equation has described the flexure of a thin plate, with " $T_e$ " corresponding to the normal thickness of the plate. The elastic thickness was introduced by applying the concept of flexural rigidity to the geological science. (In the other disciplines e.g. physics, architecture ... this parameter corresponds to a thickness of a plate.) However, to proof this assumption, the knowledge of the Young's modulus distribution and consideration of the temperature is essential.

Therefore, the elastic thickness can be defined as equivalent plate thickness, which corresponds to a plate with a constant Young's modulus. The variation of  $T_e$  can be explained by temperature distribution and a change of the Young's modulus.

The  $T_e / D$  distribution correlates very well with geological features (see chapter 3). This can be explained through the change in rigidity but also the change in Young's modulus by which geological features are characterized.

The future directions are to estimate the rigidity distribution in smaller areas, where it is sufficient to operate with a constant value for the Young's modulus and a known crustal depth  $T_c$  instead of  $T_e$  as input parameter.

Furthermore, in the original differential equation a temperature moment is considered. The solution for the temperature moment needs further investigations and calibrations. In future, the results from heat flow measurement should be considered within the area of investigation. The advantage of the analytical solution and the convolution methods is the  $T_e / D$  estimation for a small area. Only the topography is required to be known over a larger area (this is driven by the flexure parameter  $\beta$ )

This method provides many possibilities for application, because of its simplicity. Due to the fact that only the long wavelength part of the gravity field is required for the analytical solution, satellite observations can be used. An area in which this method can be applied is in the field of remote sensing.

A further future direction is the application of the investigation results of the Curvature method (PERS. COMM. KOLLERSBERGER). From the investigation of the rigidity distribution using Curvature methods a correlation with the fault structures and tectonic features can be obtained.